FINITE ELEMENT MODELLING OF STATIC LIQUEFACTION TRIGGERING MECHANISMS AND EVALUATION OF FACTOR OF SAFETY

Jiaxi (Joshua) Chan[1], Qian Gu[2]

[1] *GHD Pty Ltd, Sydney;* [2] *GHD Pty Ltd, Perth*

https://doi.org/10.56295/AGJ6046

ABSTRACT

Static liquefaction risk is one of the major risks faced in Tailings Storage Facilities (TSFs), primarily due to the contractive and strain-softening nature of loosely deposited tailings. The safety margin against the triggering of static liquefaction is difficult to evaluate using conventional Limit Equilibrium Analysis (LEA), which considers either the peak or the residual strength (assuming liquefaction has triggered). In contrast, numerical methods such as Finite Element Method (FEM), offers deeper insight by capturing the full mobilisation process beyond failure, offering a more intuitive understanding of the available safety margin. This paper presents a case study of liquefaction triggering assessment conducted as part of the design process for a TSF.

Static liquefaction simulations in Plaxis commonly utilise static analyses with an automatic unloading approach to address strain-softening numerical issues. However, this unloading (strain-controlled) approach differs fundamentally from real-world load-controlled failure mechanisms. To more accurately capture load redistribution and failure propagation during liquefaction triggering, this study adopts dynamic analysis as a more realistic method for simulating progressive failure. This paper employs dynamic analyses to clearly visualise the disturbance thresholds associated with three triggering mechanisms: undrained surface surcharge, increase of phreatic level, and toe excavation. The stress-strain behaviour for each mechanism is examined in detail.

A new definition of Factor of Safety (FoS) is evaluated for each triggering mechanism, based on changes in both deviator stress (q) and mean effective stress (p') required to trigger failure and their equivalency around the instability ratio. This offers a dimensionless alternative (therefore less dependent on the TSF size) to the conventional threshold disturbances for assessing the adequacy of safety against liquefaction.

The analyses are based on the NorSand constitutive model developed within Critical State Soil Mechanics (CSSM), and the limitations of such analyses are also discussed.

1 INTRODUCTION

Static liquefaction has been identified as a major mechanism causing catastrophic failures of Tailings Storage Facilities (TSFs). Due to the complexity of triggering analysis for static liquefaction, the conventional approach is to conservatively assume liquefaction occurs, and then adopt the residual strength of the materials in Limit Equilibrium Analysis (LEA) against a low FoS target, such as 1.1. However, this approach overlooked the potential disturbing efforts required (the safety margin) to overcome the threshold for initiating the flow failure, potentially leading to excessive conservatism. In addition, the philosophy behind this approach is not consistent with the one widely adopted in seismic liquefaction triggering assessment, which is essentially just one of many potential triggering mechanisms. For the seismic case, the liquefied residual strength is only applied in the stability assessment if the seismic disturbance is considered sufficient to trigger failure. Despite significant uncertainties associated with the seismic triggering assessment (comparable to those in static mechanisms), ranging from uncertainties of seismic events to material behaviours, such seismic triggering assessments have been widely adopted in practice. As such, it is considered valuable to conduct static liquefaction triggering analyses despite the uncertainties and limitations that exist for such works.

Numerical analyses such as the Finite Element Method (FEM) or Finite Difference Method (FDM) with appropriate constitutive models, are capable of capturing the strain-softening process of contractive tailings and have been widely undertaken by numerous researchers and engineers (Arroyo, M. and Gens, A., 2021; Babaki and Tannant, 2024; Katebi and Li, 2024; Ortigao et al. 2024; Rivas et al. 2023; Rivarola et al., 2022; Rivarola and Tasso, 2024; Rógenes et al. 2025; Rousé, 2024; Shuttle et al., 2022; Sottile et al., 2020; Vargas-Moreno et al. 2023). Some of the most significant analyses were conducted during forensic investigations following major TSF failures (Jefferies et al., 2019; Morgenstern et al., 2016; Robertson et al., 2019), utilising software packages such as Plaxis and FLAC, along with constitutive models like NorSand and the Clay and Sand Model (CASM). FLAC, with its dynamic time-marching and artificial damping approach, is generally considered numerically more capable of handling the strain softening failure process than Plaxis, although the latter has greatly improved its capability since 2011 through the introduction of automatic unloading and arc-length

control. Plaxis features a highly user-friendly interface, which may contribute to its widespread adoption particularly among practicing geotechnical engineers, including the authors of this paper, for tasks such as static liquefaction triggering analyses (Arroyo, M. and Gens, A., 2021; Babaki and Tannant, 2024; Jefferies et al., 2019; Ortigao et al., 2024; Rivas et al., 2023; Rivarola et al., 2022; Rivarola and Tasso, 2024; Rógenes et al., 2025; Shuttle et al., 2022; Sottile et al., 2020; Vargas-Moreno et al. 2023).

Most of the Plaxis-based liquefaction triggering analyses referenced above are static simulations that rely on automatic unloading to capture strain-softening failure and post-failure behaviour. While it is numerically efficient, such an approach is essentially strain-controlled by reducing or reversing load increments to maintain equilibrium, which differs significantly from the real-world failure mechanisms that are typically load controlled (e.g. surface surcharge, phreatic level increase, etc.). This discrepancy in the simulation approach may introduce uncertainties in the load redistribution and the failure propagation, both of which are critical for identifying the triggering threshold. Rivarola and Tasso (2024) adopted the static fully-coupled analyses in order to capture the rate-dependent partial drainage during failure process. Without modelling the failure process dynamically, however, the timeframe of the failure process which affects the drainage conditions may not be simulated realistically. Considering that the progressive failure is inherently a dynamic process, the dynamic analysis approach adopted by this study is considered a more realistic method of simulating the liquefaction triggering process, which aligns with the approach published by the authors of this paper in 2020 (Gu and Chan, 2020).

To utilise triggering analyses as a design tool for the proposed TSF, a dimensionless Factor of Safety (FoS) against liquefaction triggering is considered important. While several researchers and engineers have proposed such approaches (Katebi and Li, 2024; Ortigao et al., 2024; Rógenes et al., 2025), notable inconsistencies remain in both the definitions and methodologies used to estimate FoS values. For example, Ortigao et al. (2024) used a built-in strength reduction method (c-phi') to estimate the FoS against liquefaction triggering, resulting in significantly higher values compared to those from the LEA. In the authors' view, this c-phi' reduction approach does not neither realistically simulates the triggering disturbing process nor considers the undrained conditions and is therefore unlikely to offer an appropriate estimation of FoS. Rógenes et al., (2025) suggested the use of the inverse of the ratio between η (mobilised stress ratio) andM_θ (critical state stress ratio) as a "local" FoS, which may be more indicative of the final post-failure condition than the actual triggering point of liquefaction. Using a ratio relative to the instability ratio, which has been proposed by some studies (e.g. Katebi and Li, 2024), may be analogous to adopting a peak shear strength in LEA and overlooking the progressive mobilisation of stress. In this study, a new definition for the Factor of Safety (FoS) in liquefaction triggering analysis is proposed as the stress ratio between the current stress condition and the mobilised condition at the point of triggering. This definition offers the advantage of being applicable across various triggering mechanisms, unlike some other alternative definitions, such as those based on critical height or gravity over the current values (Rógenes et al., 2025), which are not suitable for mechanisms involving toe excavation, foundation deformation, increase of phreatic condition, etc.

In this study, the NorSand constitutive model, first introduced by Jefferies (1993), was used in the analyses. The derivation of the NorSand parameters (including in-situ state parameters) was conducted through interpretation of both Cone Penetration Test (CPT) and laboratory triaxial testing, following the methodology outlined by Shuttle and Jefferies (1998). NorSand is based on fundamental concepts of the Critical State Soil Mechanics (CSSM), and it uses the state parameter (the difference between the void ratio and its critical value at the current stress) as a key controlling variable to effectively capture the strain-softening process of contractive tailings.

This study uses a TSF located at McArthur River Mine (MRM) as a case example to demonstrate the methodology of static liquefaction triggering analyses. In addition to the undrained surface surcharge triggering mechanism previously simulated by authors of this paper (Gu and Chan, 2020), triggering mechanisms of phreatic level increase and toe excavation are also presented in this study. The analyses were conducted using Plaxis 2D and incorporated the NorSand constitutive model calibrated via version 18 of Visual Basic for Applications (VBA) spreadsheet (Jefferies and Been, 2016). The embankment construction and tailings deposition stages before the liquefaction triggering were first modelled with static analyses in stages to establish realistic in-situ stress conditions. The static liquefaction triggering processes were then simulated by dynamic FEM.

2 BACKGROUND

MRM comprises two TSF cells, Cell 1 (northern) and Cell 2 (southern). The tailings slurry has been historically discharged from the embankment perimeter with the decant pond located at the centre of the cells. A typical cross-section of the TSF is presented in **Figure 1**, which comprises a starter dam and subsequent upstream raises. Two zones of tailings have been considered in the model based on the different densities interpreted from available investigation data. Although the mud farming technique has been recently implemented to improve the density of tailings above RL 10060 m, such improvement has not been considered in the model due to the lack of available data and for conservatism.

Two buttress configurations have been presented in **Figure 1**, namely the interim buttress (crest at RL 57 m) and the ultimate buttress (crest at RL 60 m), respectively. The configurations were established through LEA, with FoS of 1.6 (peak strength) and 0.9 (residual strength) for the interim buttress, and FoS of 1.9 (peak strength) and 1.1 (residual strength) for the ultimate buttress. The site has a low seismicity of 0.06 g Peak Ground Acceleration (PGA) at 1 in 10,000 Annual Exceedance Probability (AEP), and the interim buttress was found to provide sufficient stability under seismic conditions. In order to further clarify the risks of liquefaction triggering during the construction period when only the interim buttress has been completed (residual strength FoS< 1.1 target), the FEM triggering analyses were undertaken for undrained surface surcharge, phreatic level increase and toe excavations triggering mechanisms.

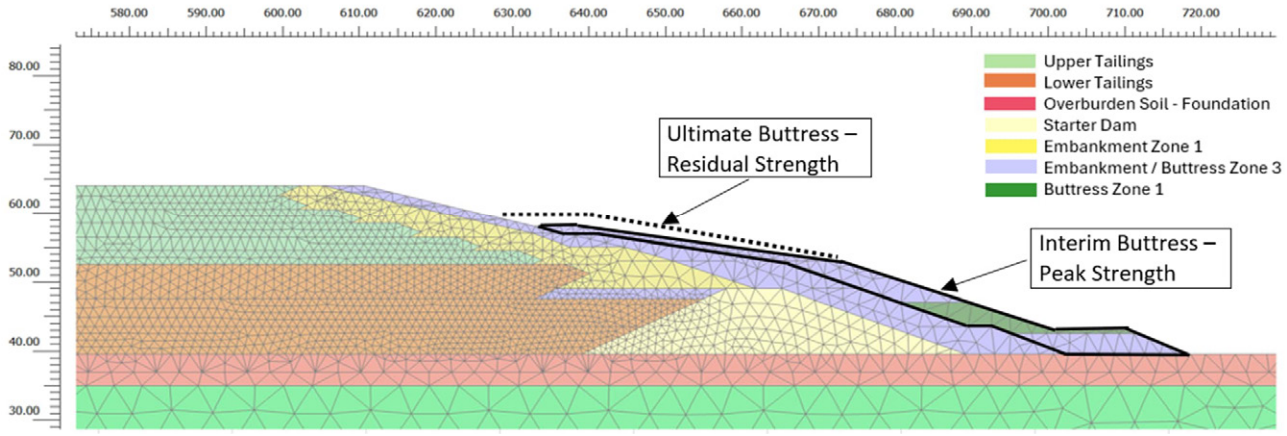

Figure 1: Typical cross section – TSF Cell 2 at MRM

3 MATERIAL PARAMETERS

3.1 TAILINGS MATERIALS

3.1.1 In-situ stress stage – Hardening Soil model

The tailings materials are generally classified as low-plasticity SILT with 70% to 85% fines, a plasticity index of 6 to 10, and a specific gravity (Gs) of 3.08 to 3.36. For the simulation stages before the liquefaction triggering process, the Hardening Soil (HS) model developed by Schanz et al. (2019) was used for the tailings materials due to its numerical stability in modelling the activation of tailing layers. The HS model parameters were selected based on the in situ and laboratory tests, as summarised in **Table 1**.

Table 1: HS soil parameters for tailings in pre-triggering stages

Material	Saturated unit weight (kN/m^3)	Effective friction angle (deg)	Effective cohesion (kPa)	$E'_{50, ref}$ (MPa)	$E'_{oed, ref}$ (MPa)	$E'_{ur, ref}$ (MPa)	Modulus dependency exponent m	Reference pressure (kPa)	K_0
Upper Tailings	23	34	0	2.5	3	9	0.6	100	0.65
Lower Tailings	23	34	0	1.5	1.5	4.5	0.6	100	0.60
Note	$E'_{50, ref}$ and $E'_{oed, ref}$ and E'_{ur} are the 50% strength Young's Modulus, Constrained Modulus and Unloading Modulus respectively, under 100 kPa reference effective confining pressure								

3.1.2 Triggering process – NorSand soil model

The Critical State Line (CSL) testing, comprising multiple undrained and drained triaxial compression tests on reconstituted samples, has been undertaken to obtain the parameters for the NorSand model (Jefferies and Been, 2016) as presented in **Table 2**. The parameters have been validated by comparing the numerically predicted undrained triaxial test results using the VBA spreadsheet (version 18) against the measured results, as shown in **Figure 2**.

It is worth noting that the G_{max} calibrated against the laboratory triaxial tests are consistently smaller (from 90% smaller in loose tests to 50% smaller for dense tests) compared to the shear wave velocity values measured from seismic CPTs. This is, however, consistent with the observations made by Shuttle and Jefferies (2016) and may be attributed to the strain rate and/or viscosity effects on the G_{max} calculated from seismic CPTs.

The in-situ State Parameters were adopted as 0.15 and 0.23 for upper and lower tailings based on the CPT results using the method recommended by Plewes et al. (1992) as shown in **Figure 3** (left). The 75th percentile of the State Parameter value was adopted. The estimated NorSand parameters have also been used in simulating 1D consolidation tests to estimate the K_0 values, which are generally within the range of values (0.5-0.7) adopted by panel reviewers for other TSF projects (Reid et al., 2021). The relationship between instability stress ratios and the state parameters was also computed from the Norsand VBA code, as shown in **Figure 3** (right).

Table 2: NorSand parameters for tailings

Material	Slope of CSL, λ_{10}	Reference void ratio Γ	Critical state q/p' ratio M_{tc}	Volumetric coupling, N	Dilatancy coefficient χ	Plastic hardening modulus H_0	Rate of change in hardening modulus H_ψ	G_{max} at 100 kPa (MPa)	Dependency exponent of G_{max}	Over-consolidation Ratio (OCR)	Softening parameter S	State parameter ψ
Upper Tailings	0.26	1.40	1.41	0.22	4.0	91	720	1.77	0.6	1.0	1.0	0.15
Lower Tailings	0.26	1.40	1.41	0.22	4.0	91	720	1.11	0.6	1.0	1.0	0.23

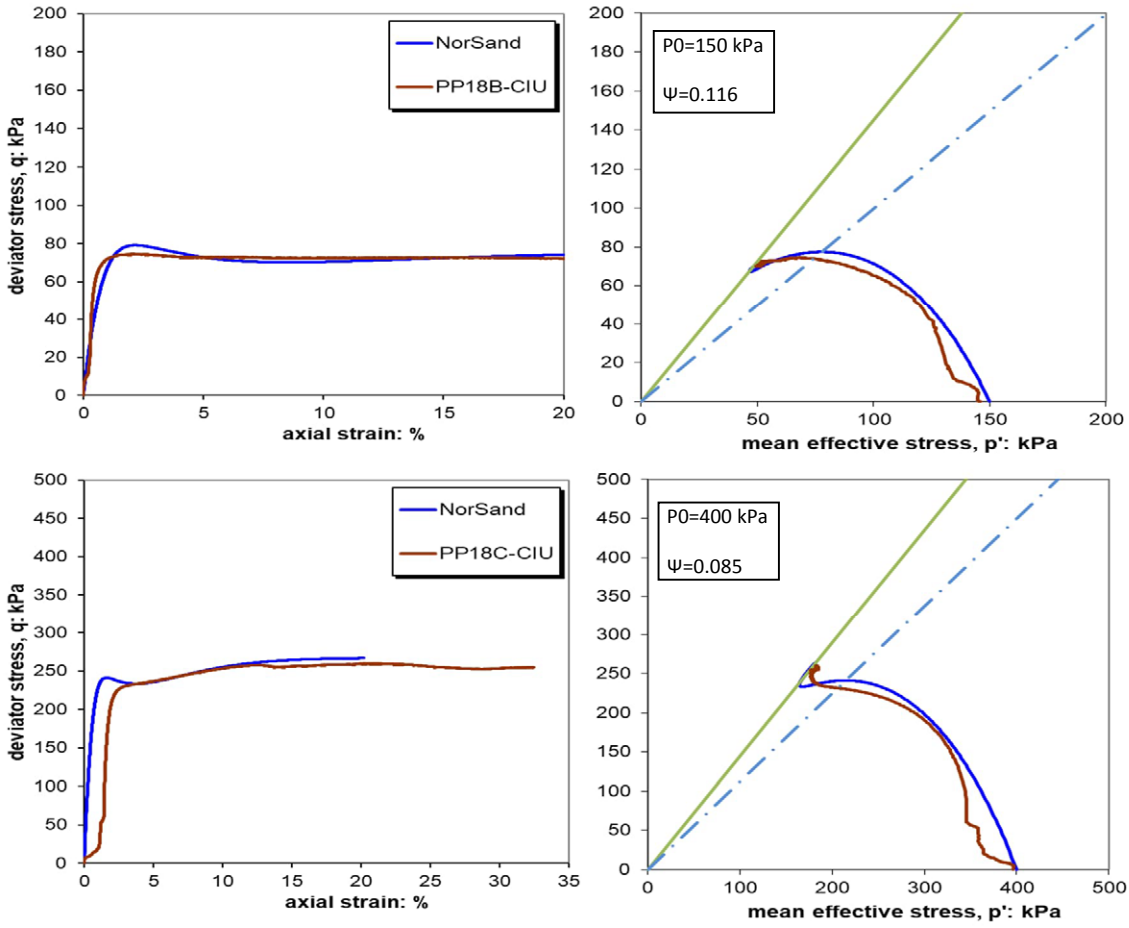

Figure 2: Undrained triaxial results from NorSand (Jefferies and Been, 2016 – version 18) against the measured data

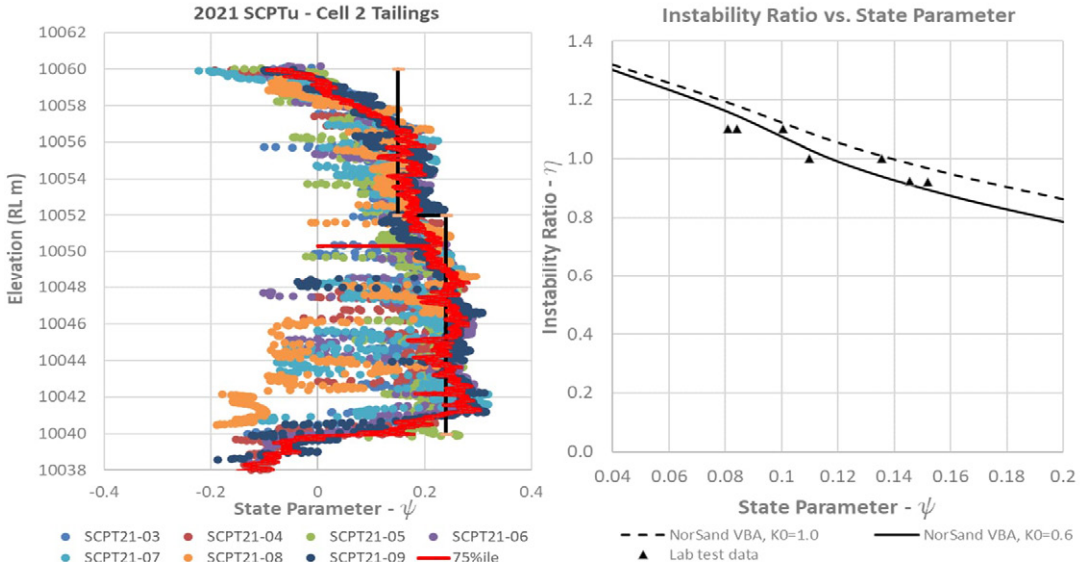

Figure 3: State parameter inferred from CPT (left) and instability ratio versus state parameters (right)

3.2 OTHER MATERIALS

The embankment and foundation materials are simulated with the Hardening Soil model (Schanz et al., 2019), for which the parameters are summarised in **Table 3**. The parameters are estimated from either geotechnical investigation information or material selection and construction specifications.

Table 3: Non-tailings material parameters

Material	Bulk unit weight (kN/m)	Effective friction angle (deg)	Effective cohesion (kPa)	$E'_{50,ref}$ (MPa)	$E'_{oed,ref}$ (MPa)	$E'_{ur,ref}$ (MPa)	Modulus dependency exponent m	Reference pressure (kPa)
Embankment / Buttress - Zone 1	20	33	0	30	30	90	0.5	100
Starter Dam	20	28	0	30	30	90	0.5	100
Embankment / Buttress – Zone 3	21	40	0	50	50	150	0.5	100
Overburden Soil – Foundation	21	28	0	20	20	60	0.5	100

3.3 DAMPING RATIO

The viscous Rayleigh Damping has been adopted to avoid eternal oscillation. A Rayleigh Damping ratio of 5% at two discrete frequencies of 0.1 Hz and 1 Hz, has been applied in all materials in the dynamic triggering analyses. The exact values of the damping ratio in the triggering analyses, however, are considered to have minor significance because the analyses are more about finding the thresholds between stable (static) and dynamic (failure) conditions, rather than accurately capturing the post-failure velocity and run-out distance, etc.

3.4 PHREATIC CONDITIONS BEFORE TRIGGERING

The pore pressure conditions of the tailings used in the FEM analysis were established by simulating the consolidation process during staged tailings deposition, as illustrated in **Figure 4**. Given that the decant pond is located over 500 meters away and the foundation is relatively permeable (10^{-6} to 10^{-8} m/s) compared to the tailings material (10^{-8} to 10^{-9} m/s), the pore pressures observed within the tailings are likely attributable mainly to consolidation effects.

Multiple suites of piezometer data and CPT dissipation test results were available within the tailings at various chainages along the embankment wall, with the representative locations shown in **Figure 4**. The maximum measurements from each suite at various chainages were superimposed in **Figure 4** for comparison. The simulated pore pressure conditions within the tailings were generally conservative relative to the piezometer measurements, and the contours were broadly consistent with the expected downward drainage behaviour.

The high pore pressure within the starter dam was caused by the high phreatic line adopted at the toe for conservatism due to the lack of piezo data here at the time of the analysis, and the historical proximity of the pond to the embankment 12 years ago at a lower elevation. The recent piezo readings have indicated negligible pore pressure at this location, confirming the conservatism. Phreatic line for the foundation was also conservatively adopted at the foundation surface level (RL 40 m).

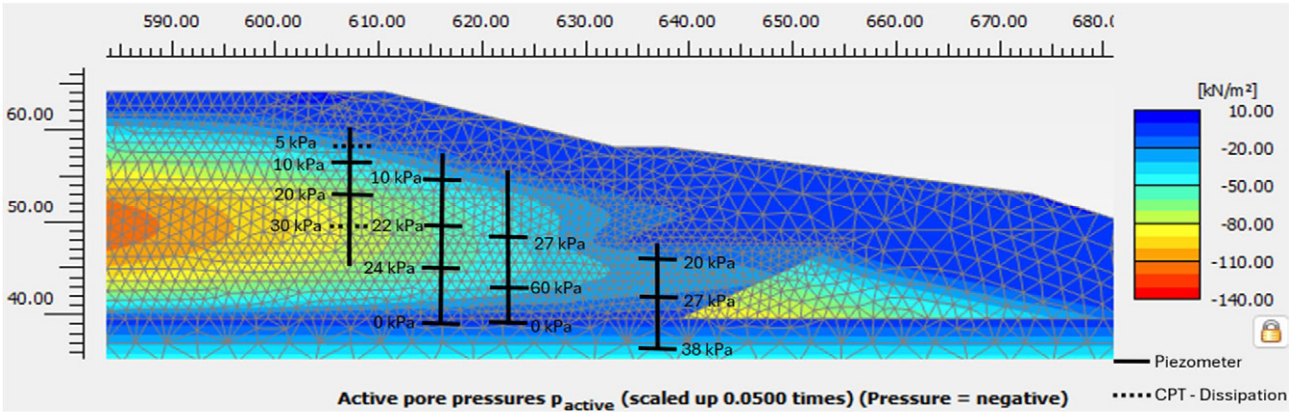

Figure 4: Pore pressure condition of tailings before the triggering process

4 TRIGGERING MECHANISM 1 – UNDRAINED SURFACE SURCHARGE

4.1 METHODOLOGY OF MODELLING

For this triggering mechanism, the procedure followed the methodology provided by the authors of this paper published in 2020 (Gu and Chan, 2020). A series of undrained surface surcharge stages, as shown in **Figure 5**, was modelled by dynamic analysis without considering the consolidation. The surcharge was increased in multiple stages and applied over the whole upper surface of the tailings. For each stage, the pressure was ramped up linearly by 10 kPa at a rate of 1 kPa per second and then held constant for 50 seconds for each stage. The duration of the constant pressure stages was selected to be adequately long to minimise any dynamic oscillations while still limiting the model run time to a manageable level.

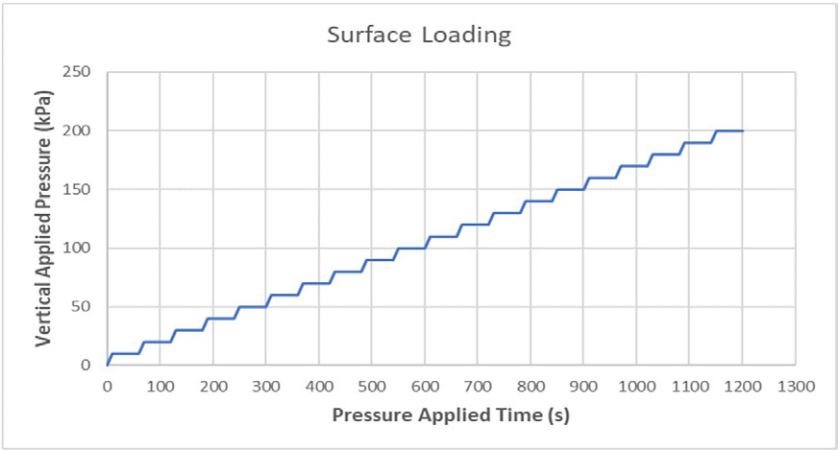

Figure 5: Time history of undrained surface disturbance pressure

To capture the failure process, multiple output points were selected along the downstream embankment surface, referenced by embankment elevation levels, to monitor the displacement. Four of these output points, which are discussed in the subsequent results, are indicated exclusively in **Figure 6**. Slip circles have also been selected along the surfaces defining the boundary of the instability zone (indicated by the concentration of shear strain) to visualise stress paths and shear resistance under different undrained surface loadings.

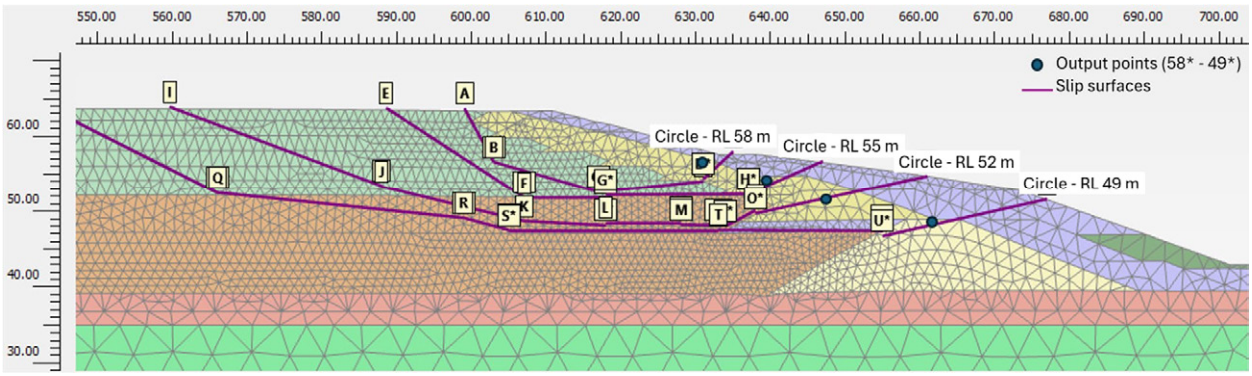

Figure 6: Cross-section with locations of slip circles and output points at different levels (RL 64 to 45 m)

4.2 THRESHOLD TRIGGERING FAILURE – UNDRAINED SURFACE SURCHARGE

Triggering of failures at different elevations can be visualised clearly by the abrupt increases of displacement and non-zero velocity under a constant stage of surface surcharge. The corresponding surface pressure that starts to cause such instability is interpreted as the threshold pressure triggering liquefaction failures. Displacement at each output point along the embankment surface is presented in **Figure 7**. The thresholds of surface surcharge versus elevation of the failure surface (exit point at embankment surface) are shown in **Figure 8**. The minimum triggering pressure is estimated to be 70 kPa for shallow slip surfaces and increases with the depth of the failure surfaces.

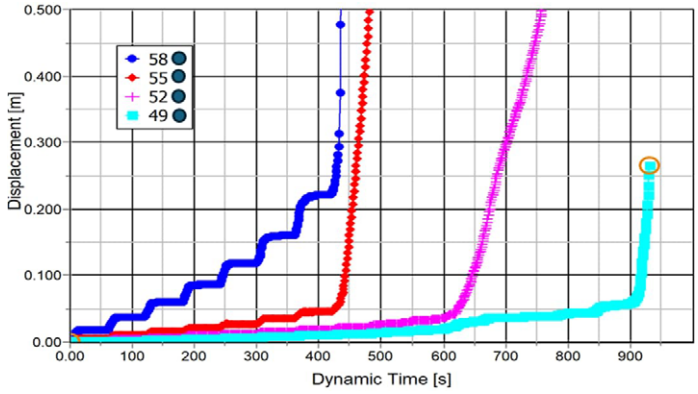

Figure 7: Displacement under different surface surcharge loads

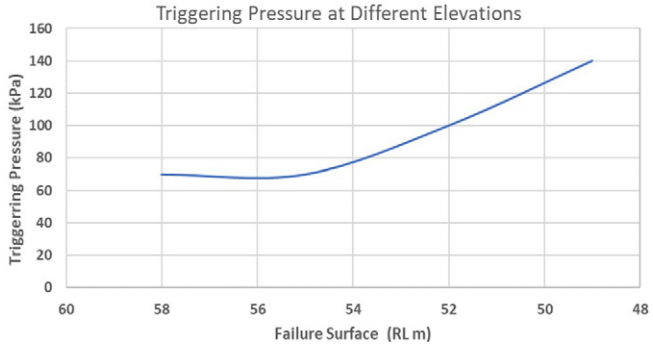

Figure 8: Threshold triggering surface surcharge vs. elevation of failure surface

4.3 STRAIN SOFTENING AND PROGRESSIVE FAILURE

To illustrate the strain softening and progressive nature of the failure caused by undrained surface surcharge, the deviator stress versus effective mean stress paths (q-p') and deviator stress (q) versus shear strain along "slip circle - RL 58 m" (location indicated in **Figure 6**) are presented in **Figure 9**. The following can be seen from the figures:

- At the completion of the drained embankment raise and tailing deposition stages, the q/p' stress ratio (η) is lower than the instability stress ratio (the ratio between peak undrained q and the corresponding p'), which is around 0.8, as expected for the embankment in a stable condition.
- Under the undrained surface loading triggering process, the mobilised q/p' stress ratio (η) increases significantly, accompanied by the consistent reduction of p' (suggesting increasing excess pore pressure), resulting in the q-p' path swerving sharply toward the Instability Line (the collapse line at the peak strength introduced and used by authors (e.g. Lade and Pradel, 1990; Ishihara, 1993; Chu and Leong, 2002; Lade and Yamamuro, 2010);
- Once the tailings are loaded beyond the instability ratio, strain softening starts, with the deviator stress (q) reducing while shear strain continues to increase, both towards the critical state condition.

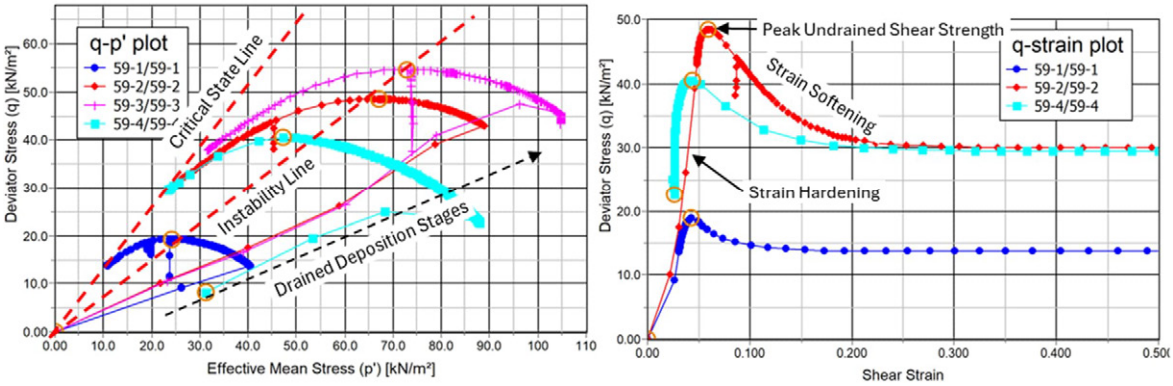

Figure 9: q-p' plot (left) and q-strain plot (right) along "circle - RL 58 m"

Figure 9 shows the development of strain-softening at the element level. The evolution of the strain-softening towards the critical state in the embankment can be visualised with the q/p' stress ratio (η) normalised against the critical state friction ratio (M), with values of 1 representing the critical state. **Figure 10** shows the development of the softening zones during the undrained triggering process using the interim buttress configuration.

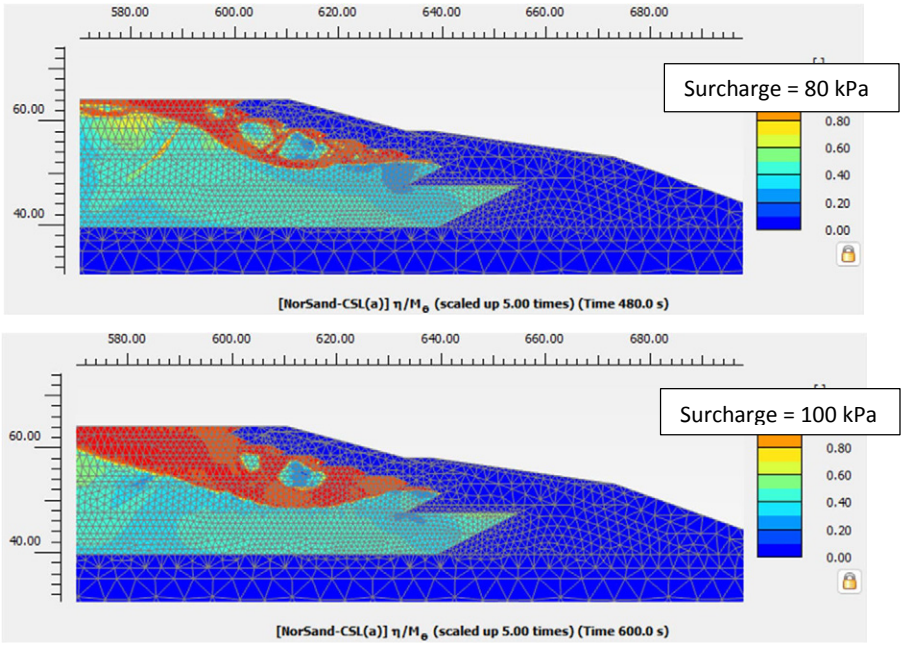

Figure 10: Evolution of softening zones within increasing surface surcharge

5 TRIGGERING MECHANISM 2 – INCREASE OF PHREATIC LEVEL

5.1 METHODOLOGY OF MODELLING

Increases in phreatic level behind the embankment, although by nature a drained process, may result in a gradual reduction of p' and shear strength towards and beyond the instability line, leading to the triggering of a brittle undrained failure. Such failures can be more abrupt compared to those induced by the surface loading described in the preceding sections, due to the lack of loading increase before failure that is usually accompanied by some precursory strain/deformation increase. This mechanism has been modelled as below.

The current NorSand model implemented in Plaxis 2D (version 2024.2) does not have the inner cap to capture the drained "unloading" contraction process and therefore cannot predict undrained liquefaction even with the stress state above the instability limits. The current study has instead adopted the Hardening Soil model during the drained phreatic level increase (which results in a stress state above the instability limit). The simulation was then switched to NorSand (so that the stress state was on the yield surface rather than inside it) to capture the undrained liquefaction failure. A Constant Shear Drained (CSD) element test was simulated in Plaxis to illustrate the above process, clearly demonstrating the capturing of liquefaction triggered as the mobilised q/p' stress ratio approached approximately 0.7 (**Figure 11**).

The insertion of **Figure 11** also shows that the dynamic analysis captured the full liquefaction process towards CSL, while the static one stopped soon after the failure started, as expected. This is one of the main reasons for adopting dynamic analyses in this study.

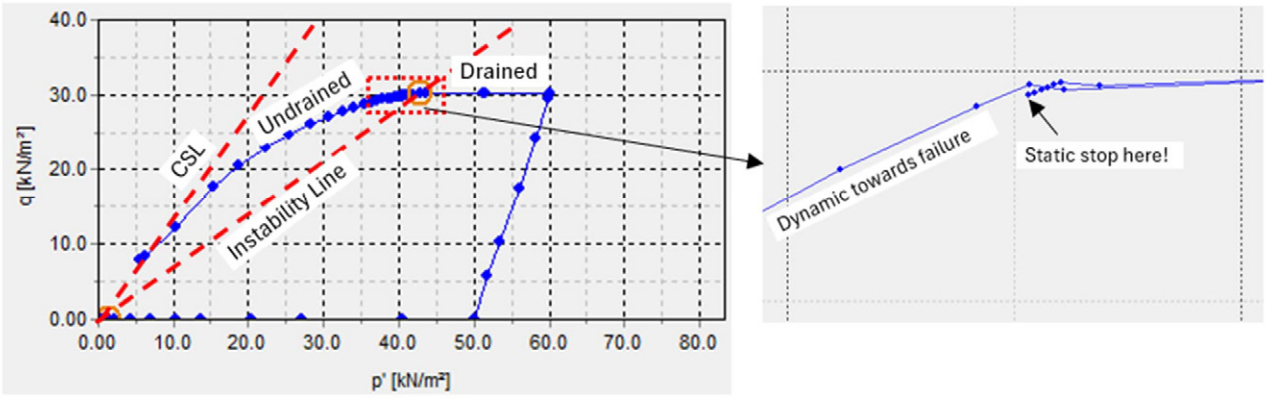

Figure 11: Element test simulated in Plaxis to illustrate unloading triggering process

In the global modelling, embankment construction and tailings deposition were the same as the static loading stages in mechanism 1. The subsequent triggering was then simulated by gradually raising the phreatic lines in multiple drained stages until it reached the upper surface of the tailings, as shown in **Figure 12**. Each raise was followed by a dynamic undrained stage using NorSand to check whether a liquefaction failure had been triggered.

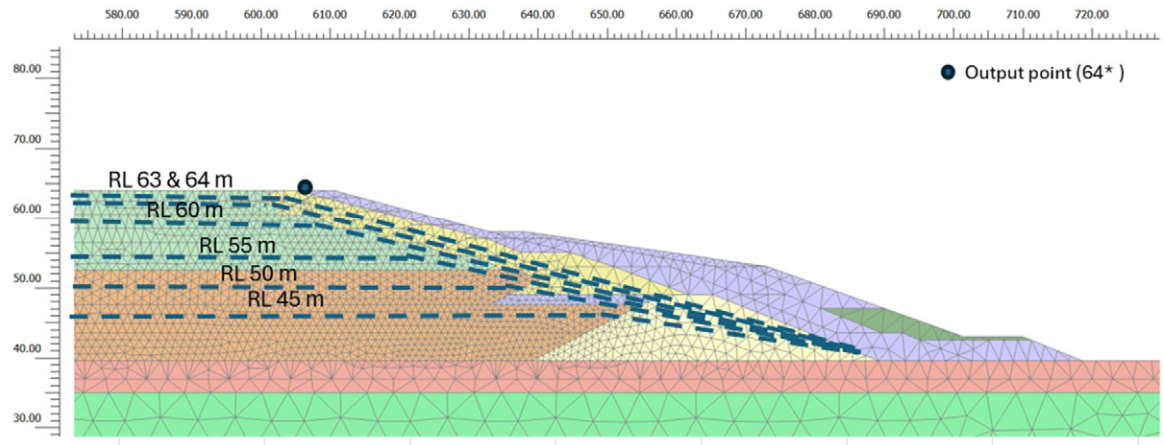

Figure 12: Increased phreatic levels to the top of TSF

5.2 THRESHOLD TRIGGERING FAILURE – PHREATIC LEVELS

The onset of liquefaction failure can be clearly visualised by the forming of a shear zone within which the displacement increases abruptly (with non-zero velocity) with the phreatic level held constant. The calculated resultant displacements from the undrained dynamic analyses corresponding to various phreatic line elevations are shown in **Figure 13**, indicating that a liquefaction failure is triggered when the phreatic level reaches RL 64 m.

The shear failure surface (indicated by the concentrated shear strain and the high stress ratio values) triggered by the phreatic level at RL 64 m is shown in **Figure 14** and **Figure 15**. Output points have been selected along the shear failure surface to capture the stress-strain behaviours prior to, during and after the triggering of the failure.

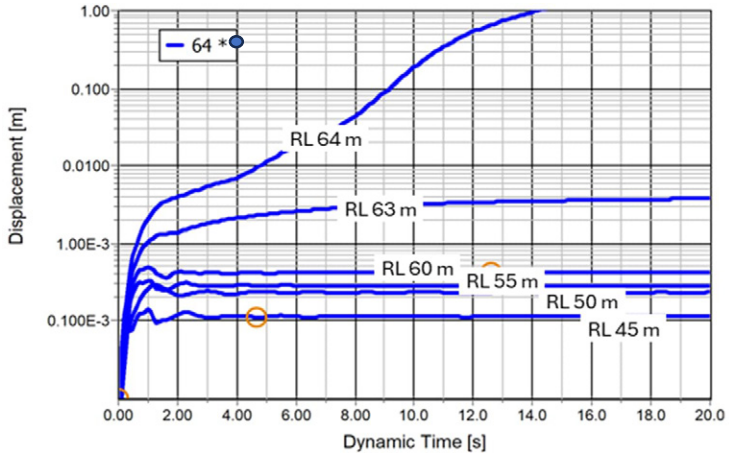

Figure 13: Dynamic displacement vs. phreatic line elevation

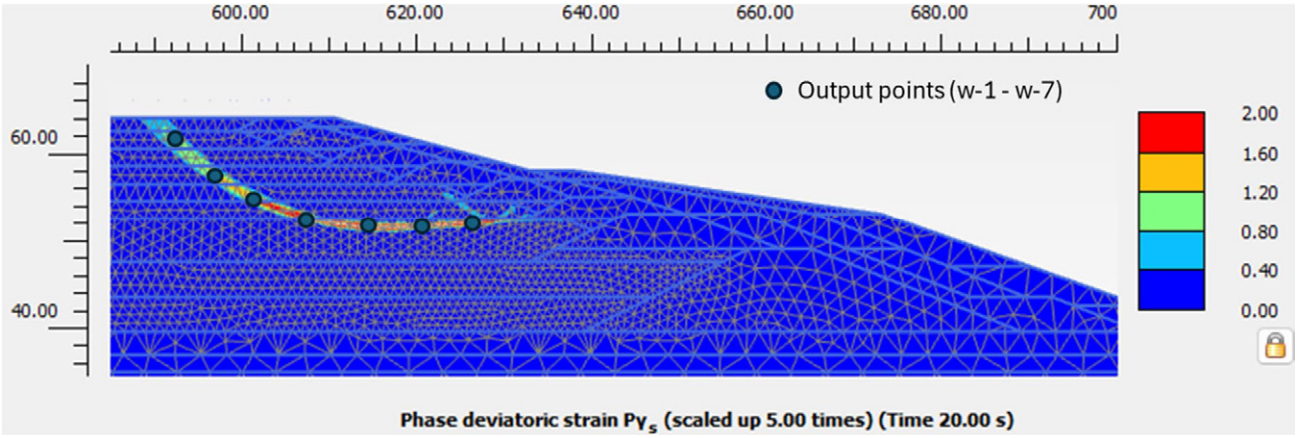

Figure 14: Concentrated shear strain defining failure surface when the phreatic line is raised to RL 64 m

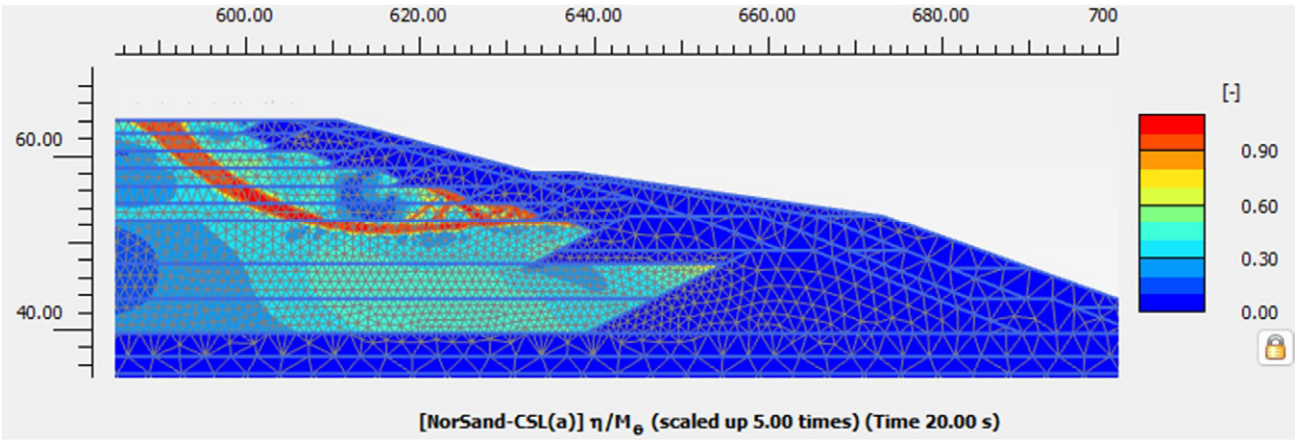

Figure 15: Stress ratio (η) against the critical state friction ratio (M) when the phreatic line is raised to RL 64 m

5.3 STRAIN SOFTENING AND PROGRESSIVE FAILURE

Similar to the surface surcharge triggering mechanism, the strain softening and progressive failure can be illustrated at the element level by examining the q-p' stress path and deviator stress (q) -strain behaviours along the failure surface, as shown in **Figure 16**. As can be seen, the increase of phreatic level results in a reduction of the mean effective stress (p'), accompanied by a mostly reduction in deviator stress q, suggesting an unloading triggering mechanism. The q versus shear strain curves show extreme brittleness of such failures, with almost no noticeable strain increase during the phreatic level rise, and instantaneous failure when the undrained dynamic mode was switched on. This failure mechanism is much more brittle compared to the undrained surface surcharge failure (**Figure 9**).

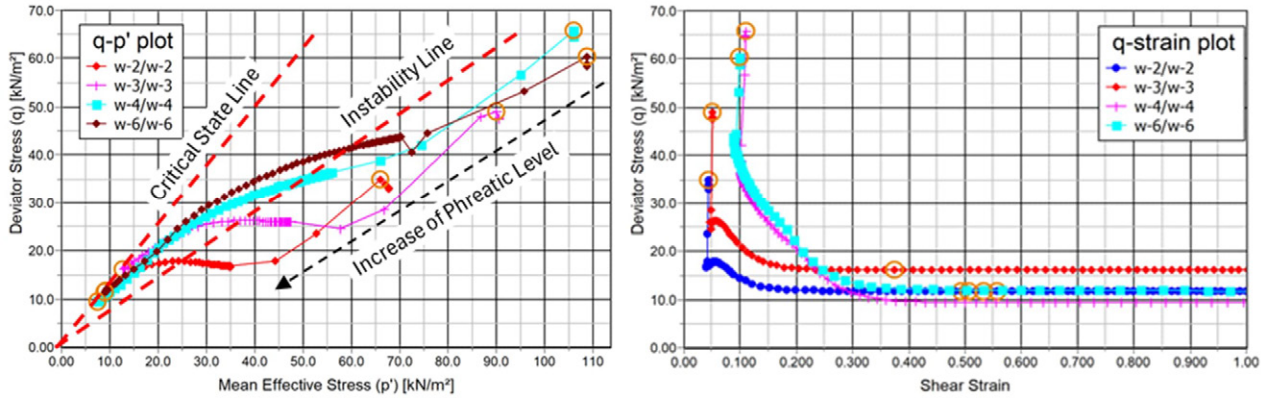

Figure 16: q-p' plot (left) and q-strain plot (right) for increased phreatic level triggering mechanism

6 TRIGGERING MECHANISM 3 – TOE EXCAVATION

7.1 METHODOLOGY OF MODELLING

Toe excavation may be required during foundation preparation works for the buttress, and the potential risk of triggering liquefaction failure by this mechanism is also evaluated using the numerical simulation. The modelling of the pre-triggering stages was the same as that discussed in previous mechanisms. The subsequent triggering was then simulated by removing the toe foundation clay layer in 1.5-meter depth intervals with an assumed batter slope of 1V:2H, as shown in **Figure 17**. A dynamic, undrained analysis stage was modelled following each stage of excavation, to check whether a failure had been triggered.

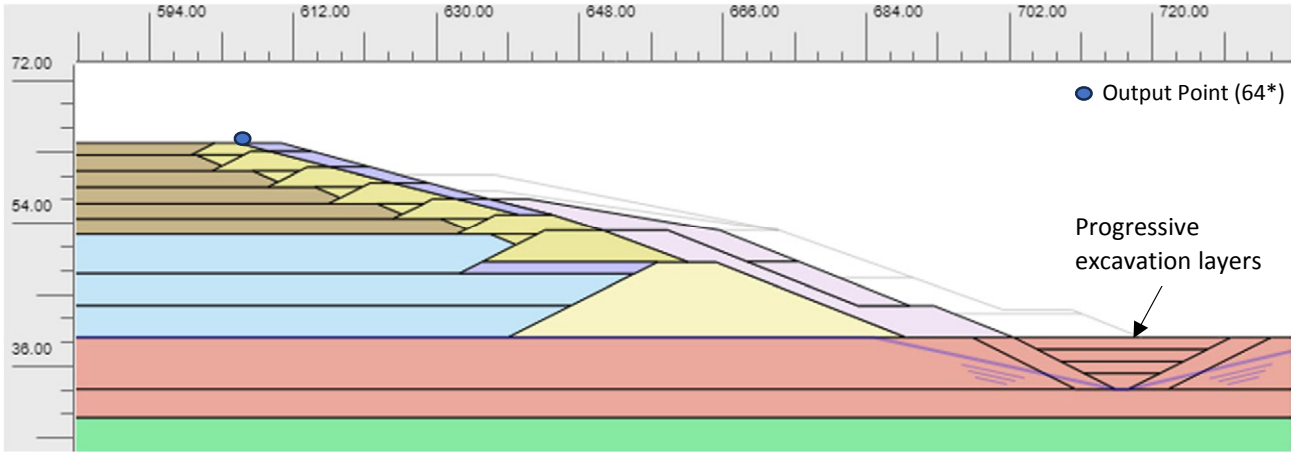

Figure 17: Toe excavation stages modelled

6.2 THRESHOLD TRIGGERING FAILURE – TOE EXCAVATION

The toe excavation mechanism in the foundation clay layer was found unable to trigger liquefaction failure due to shallow bedrock in the MRM TSF. For the purpose of illustrating the excavation triggering mechanism here, the foundation clay strength (governed by effective friction angle) has been artificially reduced from 28 degrees to 17 degrees, and the thickness increased to 10 m. As such, the results presented below are not representative of the actual conditions at MRM and potential softening behaviours of some clayey materials are also not the focus of this analysis.

The onset of liquefaction failure can be visualised by the displacement at the crest of the dam (RL 64 m) increasing abruptly (with non-zero velocity) in the dynamic analyses when the excavation depth reaches 6.5 m (**Figure 18**). The shear failure surface triggered by the toe excavation to 6.5 m is shown in **Figure 19** and **Figure 20** indicated by the concentrated shear strain and high stress ratio, respectively. A few stress points have been selected along the shear failure surface within the tailings material to illustrate the stress-strain behaviour prior to, during and after the triggering of the failure.

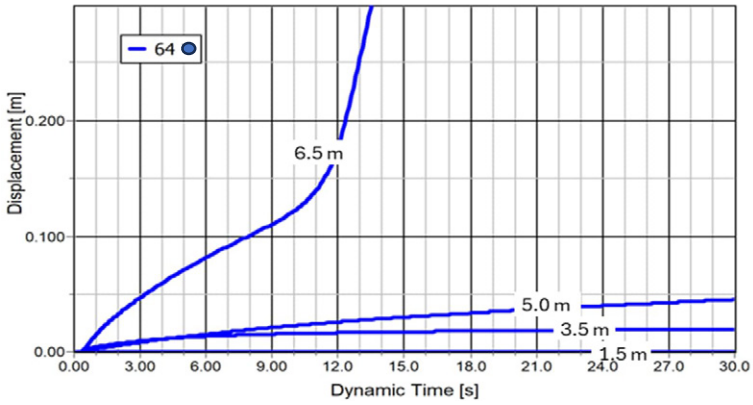

Figure 18: Dynamic displacement at crest (RL 64 m) vs. excavation depths

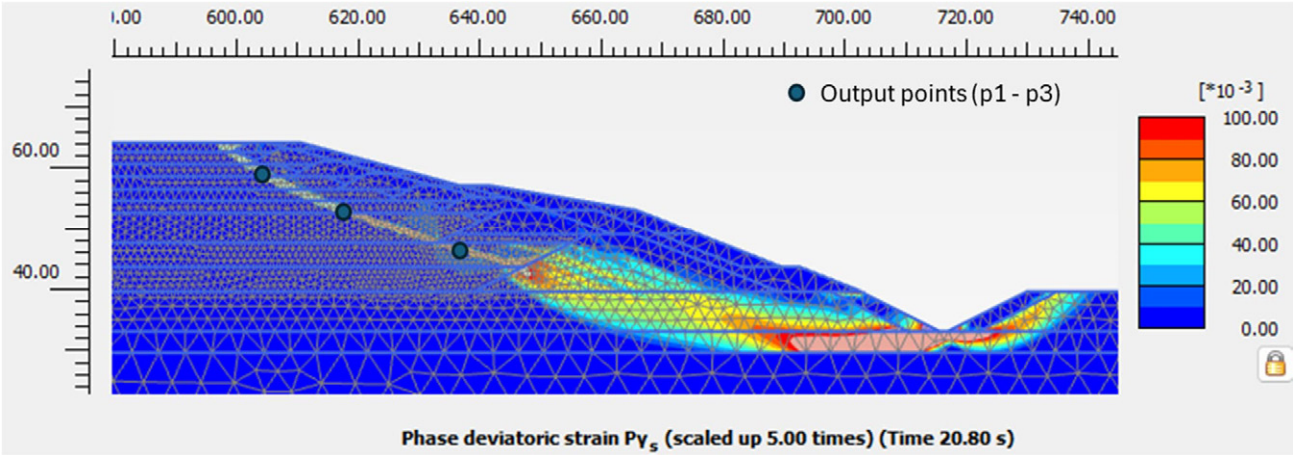

Figure 19: Concentrated shear strain defining the failure surface when the excavation depth reached 6.5 m

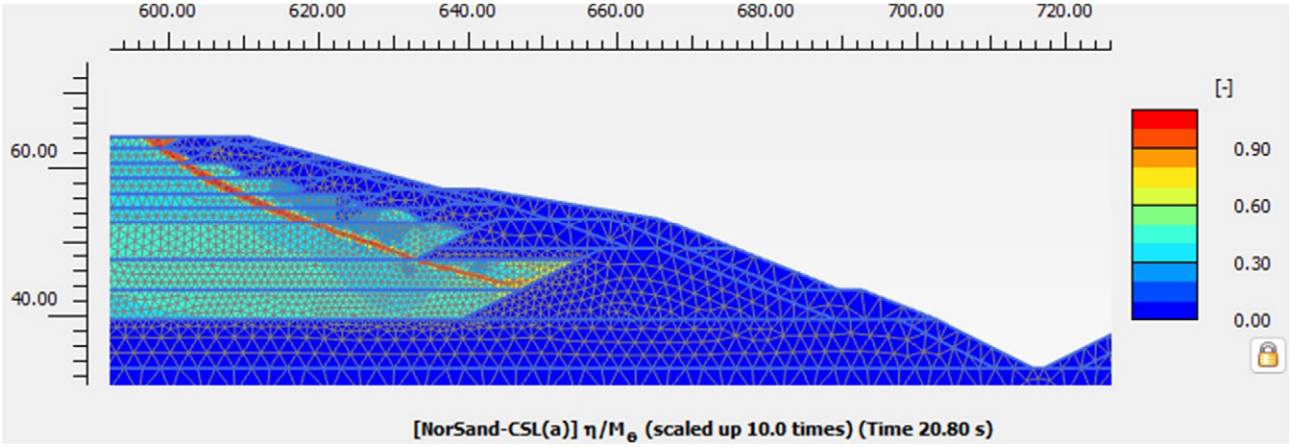

Figure 20: Stress ratio (η) against critical state friction ratio (M) when the excavation reached 6.5 m

6.3 STRAIN SOFTENING AND PROGRESSIVE FAILURE

The strain softening and progressive failure process can be illustrated at the element level by looking at the stress path and stress-strain behaviours calculated at locations along the failure surface (**Figure 21**). The toe excavation results in a slight reduction of the effective mean stress (p'), accompanied by increasing deviator stress q, pushing the q/p' stress ratio higher toward and beyond the Instability Line. Based on the pre-failure shear strain values, the toe excavation triggering seems less brittle than the phreatic level increase triggering, but more brittle than the surface surcharge one.

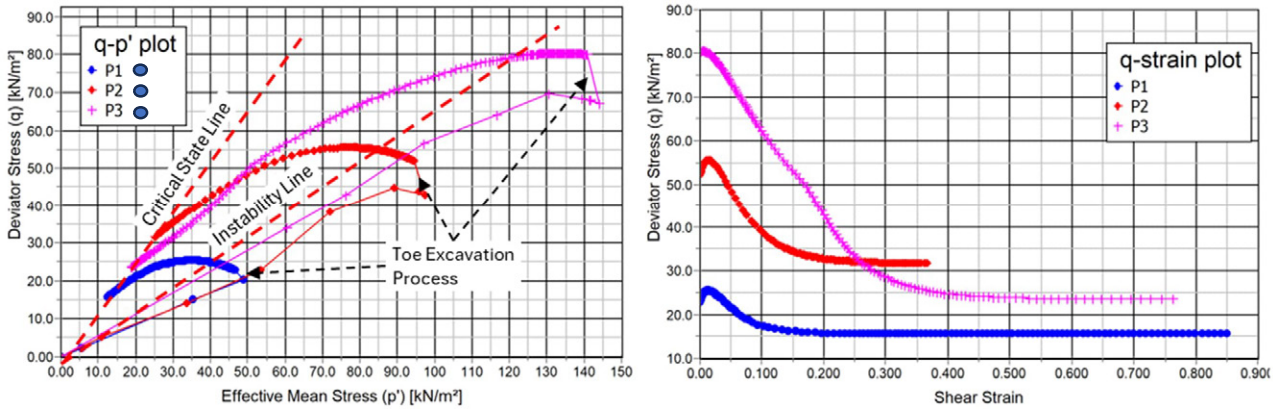

Figure 21: q-p' plot (left) and q-strain plot (right) for the excavation to 6.5 m

7 FACTOR OF SAFETY (FoS) FOR TRIGGERING

7.1 FOS VS. THRESHOLD

The preceding sections identified the threshold disturbance levels required to trigger liquefaction by different mechanisms. Although such threshold levels provide direct insight into available safety margins, one of the obvious disadvantages is their dimensional nature, expressed in units such as kilopascals for surcharge pressure, metres for the phreatic level increase and excavation depth. As a result, the same triggering disturbances do not reflect the equivalent safety margin for embankments with different scales. For example, a 5 m phreatic level increase to trigger failures implies a significantly greater safety margin for a small 5 m high embankment than for a 50 m high dam. Moreover, comparing safety levels across different mechanisms become impossible using dimensional values alone. To enable consistent evaluation of safety margins across varying TSF geometries and failure modes, a dimensionless term, such as FoS, widely adopted for LEA, needs to be defined for the FEM triggering assessment.

7.2 DEFINITION OF FOS FROM FEM TRIGGERING MODELLING PERSPECTIVE

In LEA, the FoS is simply defined as the ratio of the available resistance (strength) to the disturbing force (force) with the strength treated as a direct input parameter that remains independent to different triggering mechanisms. In contrast, for triggering assessment using FEM, the "strength" is not a direct input parameter anymore, but a result of stress-strain response controlled by the adopted effective stress parameters and the magnitude of the disturbing force imposed by different triggering mechanisms. Also, failures can be triggered not only through the loading process but also via the unloading process, where deviator stress q' reduces to trigger failure (e.g. **Figure 16**). Therefore, a new approach is proposed to estimate the FoS value for various liquefaction triggering mechanisms within FEM analyses.

The fundamental concept to derive the FoS was similar to the evaluation of safety margin to liquefaction using the instability line (e.g. Lade and Pradel, 1990; Ishihara, 1993; Chu and Leong, 2002; Lade and Yamamuro, 2010). However, unlike element-level evaluations, the FoS in this study was estimated at the average level of the slip surface. The FoS can be defined as the ratio of the available resistance (strength) to the current shear stress acting along the slip surface, as shown below.

$$FoS = \frac{R_0}{q_0} = \frac{p'_0\eta}{q_0} = \frac{p'_o\eta}{q_o} \times \frac{\frac{p'_f}{p'_f}}{\frac{q_f}{q_f}} = \frac{p'_f\eta}{q_f} \times \frac{\frac{p'_0}{p'_f}}{\frac{q_0}{q_f}} \quad \text{Eq. (1)}$$

At the failure point located on the instability line:

$$\frac{p'_f \eta}{q_f} = 1 \qquad \text{Eq. (2)}$$

The equation (1) can become:

$$FoS = \frac{p'_0}{p'_f} \cdot \frac{q_f}{q_0} \cdot \qquad \text{Eq. (3)}$$

In which:

- R_0 is resistance as defined in LEA, the deviator stress on the instability line at p'_0
- q_0 is the current deviator stress
- p'_0 is the current mean effective stress
- η is the q/p' ratio of the instability line defining the peak shear strength
- q_f is the mobilised deviator stress at the failure-triggering moment
- p'_f is the mobilised mean effective stress at the failure-triggering moment

The definitions of the above parameters are illustrated in **Figure 22** below.

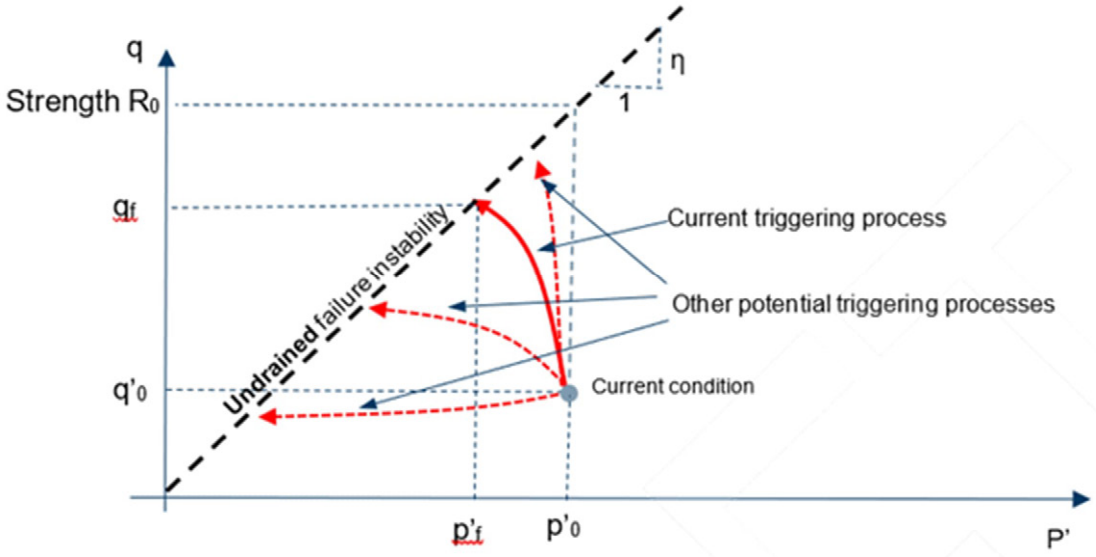

Figure 22: Schematic illustration of the meaning of parameters in Eq. (1)

Compared to the triggering analyses, the LEA defines FoS as the ratio of "shear strength" to the current shear stress without explicitly considering the change in effective stress (from p'_o to p'_f), i.e., FoS = $\frac{q_f}{q_0}$ and $\frac{p'_o}{p'_f}$=1. The "strength" (q_f) is an input parameter based on the initial effective stress (p'_o). As the LEA cannot capture shear-induced changes in effective stress p', (i.e. p'_f not computed), the effect of such changes on strength must be represented indirectly through varying strength ratios ($\frac{q_f}{p'_0}$) to reflect different stress paths. In contrast, FEM-based triggering assessment explicitly consider the evolution of effective stress p' (i.e. $\frac{p'_o}{p'_f} \neq 1$) enabling the FoS computed directly from changes of deviator stress (q) and effective mean stress (p') as outlined in Eq. (3).

When failure occurs along the whole slip surface, this definition of FoS can be applied in an average sense. The average deviator stress (q) and effective mean stress (p') can be obtained along the slip surface from the stress outputs of the FEM model. Observations indicate that the stress states of different locations at the moment of triggering failure were either above or below the instability line, which is because of the progressive nature of the failure that some points had already mobilised beyond the peak strength (crossing the instability line) while others were still undergoing hardening towards it.

7.3 FOS AGAINST STATIC LIQUEFACTION TRIGGERING MECHANISMS

Based on the above discussion and Eq. (3), FoS against surface surcharge triggering mechanisms along the embankment height are shown in **Figure 23**, together with FoS values obtained from LEA. The following can be seen from the figure:

- As expected, the FoS from triggering analyses are well within the range of the values estimated from LEA using peak and residual shear strength values.
- A general trend of FoS obtained from the triggering analysis is consistent with the LEA analysis with the lowest FoS of 1.4 obtained for slip surface daylighting the embankment elevation around RL 55 m.

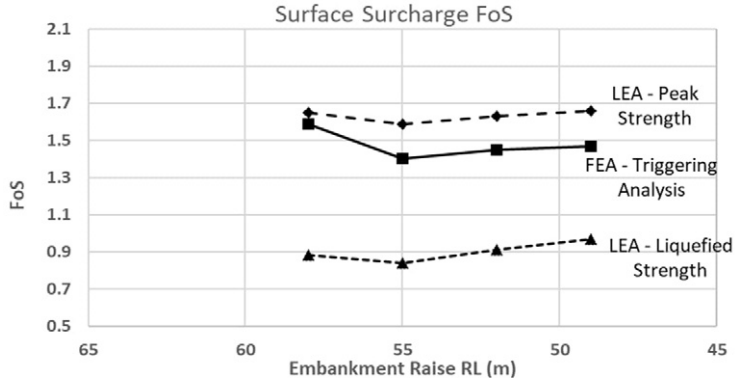

Figure 23: FoS vs embankment RL - surface surcharge mechanism

In terms of the increased phreatic level mechanism, liquefaction failure was found to be triggered when the phreatic line was elevated to RL 64 m. The corresponding slip surface daylighting at the embankment raise at RL 58 m and its FoS against triggering was calculated to be approximately **1.46**. For the same slip surface, FoS values estimated from LEM using peak strength and liquefied strength are 1.60 and 0.88, respectively. This FoS value estimated from the FEM is found to be similar to the one estimated from the surface surcharge mechanism.

As for the toe excavation mechanism, liquefaction failure was not triggered using realistic strength parameters of the in-situ foundation. In the case with the reduced strength in the foundation soils (friction angle of 17 degrees), the FoS was calculated to be approximately 1.16.

7.6 TARGET FOS FOR STATIC LIQUEFACTION TRIGGERING ANALYSES

Although not explicitly mentioned, the current minimum FoS values recommended by the Australian National Committee on Large Dams (ANCOLD) Guidelines on Tailings Dams (2019) are primarily intended for the assessments using the LEA method, and uncertainties remain regarding the applicability of the same targets to the FEM triggering analyses. To address this gap, further work is necessary from the industry to establish a standardised methodology and acceptance criteria for FEM-based triggering analyses, taking into account specific risk levels and associated uncertainties. In the interim, a target FoS of 1.5 for the triggering analyses may be considered a prudent approach for the stability of TSFs.

8 DISCUSSION AND CONCLUSION

This paper has presented the methodology and results of FEM-based triggering analyses on three potential failure mechanisms. These analyses can capture the disturbing efforts required to overcome the threshold to trigger the flow failure process, which is more realistic compared to the conventional approach assuming liquefied residual strength in LEA. Such an assumption in LEA, although conservative (if appropriate liquefied strength adopted), ignores the potential margin available against the triggering. Moreover, it is not fully consistent with the philosophy of the widely adopted seismic liquefaction triggering assessment, which evaluates the potential of triggering to inform what strength to adopt in the stability analyses.

Three static liquefaction triggering mechanisms, including the undrained surface surcharge, increase of phreatic level, and toe excavation, have been assessed in this study. For each mechanism, the required threshold levels of disturbances were identified, and corresponding dimensionless FoS values (based on a definition of q/p' ratio) have been estimated.

It shall be acknowledged, however, that significant uncertainties currently exist for the triggering analyses. One of these is whether all critical mechanisms have been adequately considered in the analyses, or whether the safety margins derived from the assessed mechanisms can reasonably serve as proxies for numerous other potential scenarios that were not explicitly investigated. One potential solutions may be to first identify critical and credible triggering mechanisms based on a comprehensive risk assessment.

As noted by Reid et al. (2021), a significant uncertainty may arise from the selection of K_0 values, which affects both the interpretation of the in-situ state parameters and the assessment of the proximity to the instability limit. Although the K_0 value in tailings is generally considered higher than the one at the normally consolidated state (~0.5) due to post-depositional disturbances (e.g. vibration due to mining activities), there remains a lack of consensus on the exact value even following in-situ testing, such as dilatometer and pressure meter tests or laboratory consolidation tests. Reid et al. (2021) also highlighted the impact of the depositional anisotropy and inclination of principal stress direction in reducing the undrained shear strength, which has not been accounted for in the current study based on the results of triaxial compression tests. Besides, the current analyses were based on strength-stress behaviour calibrated against controlled laboratory conditions, which do not fully capture complex failure mechanisms such as void redistribution, strain localisation, and intermixing during the failure processes. These limitations are common across many triggering analyses (e.g., Arroyo, M. and Gens, A., 2021; Babaki and Tannant, 2024; Katebi and Li, 2024; Ortigao et al. 2024; Rivas et al. 2023; Rivarola et al., 2022; Rivarola and Tasso, 2024; Rógenes et al. 2025; Rousé, 2024; Shuttle et al., 2022; Sottile et al., 2020; Vargas-Moreno et al. 2023). Considering these uncertainties, this study has adopted conservative assumptions for other key parameters, including pore pressure conditions and selection of state parameters.

For practical applications, all the above uncertainties condense to a question of the appropriate target FoS that shall be adopted. Establishing clear guidelines for FEM-based triggering analyses will require further industry consensus and development. In the meantime, such analyses are most likely to be applied in support of stability justification for short-term or temporary operational stages, where conservative assumptions and limited exposure durations may offer acceptable levels of risk.

Notwithstanding the aforementioned uncertainties and the need for further refinement of the analyses, the authors believe that there are intrinsic values of such triggering analyses, as demonstrated by this paper, in better understanding the risks against triggering liquefaction failures. This approach parallels the utility of more widely adopted seismic liquefaction triggering methodologies, contributing meaningfully to risk assessment and mitigation strategies.

CRediT authorship contribution statement

Jiaxi (Joshua) Chan: Formal analysis, Writing - original draft, Writing – review and editing. **Qian Gu**: Writing - original draft, Writing – review and editing.

REFERENCES

ANCOLD, 2019. Guidelines on Tailings Dam, Australian National Committee on Large Dams Incorporated, Australia.

Arroyo, M. and Gens, A., 2021. Computational analyses of Dam I failure at the Corrego de Feijao mine in Brumadinho. *Final Report for VALE SA*.

Babaki, A.P. and Tannant, D.D., 2024. Numerical evaluation of static liquefaction–induced flowslide causing the Edenville Dam failure, Michigan. *Journal of Geotechnical and Geoenvironmental Engineering*, *150*(5), p.04024034.

Bishop, A. W. (1950). Reply to discussion on "measurement of shear strength of soils" by a.w. skemptonand and a.w. bishop. Géotechnique, 2:90-108.

Chu, J. and Leong, W.K. (2002). Effect of fines on instability behaviour of loose sand. Géotechnique, 52(10), 751–755.

Drucker, D. C. (1951). A more fundamental approach to stress-strain relations. In Proceedings of the First US National Congress of Applied Mechanics, pages 487-491. ASME, ASME.

Gu and Chan (2020). Dynamic Analyses for Static Liquefaction Factor of Safety and Triggering Threshold Values in Tailings Storage Facilities Constructed by Upstream Method. 2020 ANCOLD Conference. ANCOLD.

Ishihara, K. (1993). Thirty third Rankine lecture: Liquefaction and flow failure during earthquakes. Géotechnique, 43(3), 349–415.

Jefferies, M. (1993). “Nor-sand: a simple critical state model for sand”, Géotechque 43, 91-103

Jefferies, M. and Been, K. (2016). Soil Liquefaction, a Critical State Approach. Applied geotechnics series. CRC Press.

Jefferies, M., Morgenstern, N.R., Van Zyl, D. and Wates, J., 2019. Report on NTSF embankment failure Cadia Valley operations for Ashurst Australia. *Independent Technical Review Board. Accessed May*, *1*, p.2019.

Katebi, M. and Li, S., A review of the FLAC (2D/3D) implementation of the NorSand model for static liquefaction analysis of tailings dam, 2024.

Lade, P.V. and Pradel, D. (1990). Instability and plastic flow of soils. I: Experimental Observations. Journal of Engineering Mechanics, ASCE, 116(11), 2532–2550.

Lade, P.V. and Yamamuro, J.A. (2010). Evaluation of static liquefaction potential of silty sand slopes. Canadian Geotechnical Journal, 48(2), 247–264.

Morgenstern, N.R., Vick, S.G., Viotti, C.B. and Watts, B.D., 2016. Fundão tailings dam review panel report on the immediate causes of the failure of the Fundão dam. *Cleary Gottlieb Steen & Hamilton LLP, New York*.

Ortigao, A., Sieira, A.C., Santos, F., Moraes, J. and Soares, C., 2024. Liquefaction Analysis of Four High Tailings Dams. *European Journal of Engineering and Technology Research*, *9*(3), pp.47-56.

Plewes, H.D., Davies, M.P. and Jefferies, M.G. (1992). CPT based screening procedure for evaluating liquefaction susceptibility. In Proceedings of the 45th Canadian Geotechnical Conference, Toronto, Canada.

Reid, D., Dickinson, S., Mital, U., Fanni, R. and Fourie, A., 2021. On some uncertainties related to static liquefaction triggering assessments. *Proceedings of the Institution of Civil Engineers-Geotechnical Engineering*, *175*(2), pp.181-199.

Reid D, Fanni R and Fourie A (2021) Assessing the undrained strength cross-anisotropy of three tailings types. Géotechnique Letters, https://doi.org/10.1680/jgele.21.00094.

Rivarola, L.F. and Tasso, N., 2024. Analysis of flow liquefaction triggering in tailings dams considering coupled flow-deformation. In *Proceedings of the 17th Pan-American Conference on Soil Mechanics and Geotechnical Engineering. La Serena, Chile*.

Rivarola, F.L., Tasso, N., Bernardo, K. and Sfriso, A., 2022. Numerical Aspects to Evaluate Triggering of Static Liquefaction with the HSS Model. *Mecánica Computacional*, *39*(28), pp.983-992.

Rivas, N., Sottile, M., Rivarola, F.L. and Sfriso, A., 2023. Comparing HSS and NorSand constitutive model for modeling flow liquefaction in tailings dams. In *Proc., 1st Int. Conf. on Geotechnics of Tailings and Mine Waste. London, UK: International Society for Soil Mechanics and Geotechnical Engineering (ISSMGE)*.

Robertson, P.K., L.d. Melo, D.J. Williams, and G.W. Wilson. 2019. Report of the Expert Panel on the Technical Causes of the Failure of Feijão .

Rógenes, E., Paes, I.T., Delgado, B.G., Bittar, R.J., Gomes, A.D.S., Cirone, A., Favero Neto, A.H. and Rasmussen, L.L., 2025. Assessing Static Liquefaction Triggers in Tailings Dams Using the Critical State Constitutive Models CASM and NorSand. *International Journal for Numerical and Analytical Methods in Geomechanics*, *49*(4), pp.1092-1112.

Rousé, P., Comparative analysis of P2PSand and NorSand models for static liquefaction assessment in tailings dams, 2024.

Schanz, T., Vermeer, P.A. and Bonnier, P.G. (2019). The hardening soil model: Formulation and verification. In Beyond 2000 in computational geotechnics (pp. 281-296). Routledge.

Shuttle, D.A. and Jefferies, M.G. (1998). Dimensionless and unbiased CPT interpretation in sand. International Journal of Numerical and Analytical Methods in Geomechanics, 22, 351–391.

Shuttle, D.A., and Jefferies, M.G. (2016). Determining silt state from CPTu. Geotechnical Research, 3, 90-118.

Shuttle, D., Marinelli, F., Brasile, S. and Jefferies, M., 2022. Validation of computational liquefaction for tailings: Tar Island slump. *Geotechnical Research*, *9*(1), pp.32-55.

Sottile, M.G., Cueto, I.A. and Sfriso, A.O., 2020. A simplified procedure to numerically evaluate triggering of static liquefaction in upstream-raised tailings storage facilities. *arXiv preprint arXiv:2010.11705*.

Vargas-Moreno, C.O., Guillén-Guillén, J.B., Ramírez-Chávez, R. and Preciado, H.F., 2023. Numerical Analysis for the Stress-Strain Evaluation of the Conversion of a Conventional Slurry Tailings Storage Facility to Filtered Tailings Storage Facility, Considering Different Scenarios. In *Proceedings of Tailings and Mine Waste* (pp. 29-41).